# Transfer Printing Assisted Fabrication of a Cicada Wing Inspired Nanopaper SERS Platform

Wenwen Yuan
*School of Advanced Technology, Xi'an Jiaotong-Liverpool University*
*College of Information Engineering, Shanghai Maritime University*
Suzhou, China
wwyuan@shmtu.edu.cn

Hang Yuan
*School of Advanced Technology, Xi'an Jiaotong-Liverpool University*
*Department of Biomedical Engineering, Michigan State University*
Suzhou, China
Hang.Yuan20@alumni.xjtlu.edu.cn

Eng Gee Lim
*School of Advanced Technology, Xi'an Jiaotong-Liverpool University*
*Department of Electrical Engineering and Electronics, University of Liverpool*
Suzhou, China
enggee.lim@xjtlu.edu.cn

Ivona Mitrovic
*Department of Electrical Engineering and Electronics, University of Liverpool*
Liverpool, UK
Ivona@liverpool.ac.uk

Yining Shi
*School of Advanced Technology, Xi'an Jiaotong-Liverpool University*
*Department of Electrical Engineering and Electronics, University of Liverpool*
Suzhou, China
Yining.Shi24@student.xjtlu.edu.cn

Pengfei Song*
*School of Advanced Technology, Xi'an Jiaotong-Liverpool University*
*Department of Electrical Engineering and Electronics, University of Liverpool*
Suzhou, China
Pengfei.Song@xjtlu.edu.cn

2025 International Conference on Advanced Mechatronic Systems (ICAMechS) | 979-8-3315-8730-7/25/$31.00 ©2025 IEEE | DOI: 10.1109/ICAMechS68051.2025.11181032

***Abstract*—Because of the ultrasmooth surface and high optical transparence nanostructure, nanofibrillated cellulose paper (nanopaper) has been thinking as a promising substrate material for various areas, particularly in the highly sensitive detection technique, surface-enhanced Raman scattering (SERS). Conventional SERS detection typically relies on substrates with two-dimensional structures, which are often unsuitable for analytes with low adsorption capacity. In contrast, the surface architectures found in plants and animals possess distinctive three-dimensional micro/nanostructures that can generate abundant electromagnetic hot spots, offering a bioinspired strategy for enhancing SERS signals. In this work, we develope a cicada-wing-inspired nanopaper SERS platform via an integrated transfer-printing-assisted fabrication method. Electromagnetic simulations confirmed that the replicated nanostructures facilitated hot spot formation and improved the interaction between plasmonic nanoparticles and analyte molecules. Using Rhodamine 6G (R6G) as the SERS example, the substrate achieved an exceptionally low limit of detection (286 fM) and a high enhancement factor ($1.09 \times 10^9$). These results demonstrate that the proposed fabrication strategy enables practical, high-performance nanopaper-based biomimetic SERS substrates.**

**Keywords—*Three-dimensional nanostructures, Biomimetic SERS substrates, Nanopaper-based SERS platform***

## I. INTRODUCTION

Nanofibrillated cellulose (NFC) paper (nanopaper) has emerged as a reliable substrate for diverse utilizations, including electrical and analytical device fabrication [1]-[3]. Nanopaper possesses similar characteristics to conventional cellulose paper, such as hydrophilicity, biodegradability, flexibility, and cost-effectiveness [4], [5], [6]. In the context of surface-enhanced Raman scattering (SERS), its elevated optical transparency and low haze minimize light loss, while its dense cellulose matrix and ultrasmooth surface (roughness < 25 nm) facilitate the fabrication of uniform nanostructures [7], [8], [9]. Our previous work demonstrated *in situ* growth of plasmonic nanostructures on nanopaper via redox reactions [10], [11]. However, this approach required additional chemical steps and could not directly integrate noble metal nanoparticles into the substrate.

Transfer printing has gained considerable attention as a simple, high-throughput, and low-cost nanofabrication method. It is capable of producing functional structures with two-dimensional (2D) and three-dimensional (3D) layouts on a variety of substrates, including flexible and non-planar surfaces [12], [13], [14]. This additive process enables the direct transfer of plasmonic inks such as silver (AgNPs) nanoparticles or gold nanoparticles (AuNPs) in a single step, offering both scalability and design flexibility [15]. While this method has been applied to various soft materials [16], [17], its potential for fabricating nanopaper-based SERS substrates remains unexplored. The abundant hydroxyl groups on nanopaper surfaces provide a straightforward route for surface modification, enabling efficient attachment of plasmonic nanostructures via transfer printing.

3D plasmonic architectures generally exhibit stronger SERS enhancement than 2D counterparts by increasing binding sites for analytes and generating more electromagnetic hot spots [18], [19], [20]. Solid substrates with micro/nanoscale roughness, particularly those inspired by natural surfaces such as plant leaves or insect wings, have shown remarkable SERS performance [21]. Among them, cicada wings (*Cryptotympana atrata Fabricius*) possess regularly arranged cone-shaped nanopillars that can utilize as a bioscaffold for plasmonic decoration, providing enhancement of light trapping and hot spot generation [22], [23], [24]. Therefore, the creation of cicada wings-based 3D biomimetic SERS substrates is highly desired and holds offers wide range of potential applications.

The authors acknowledge the financial support from the programs of the Natural Science Foundation of the Jiangsu Higher Education (24KJB460030), and XJTLU RDF project (RDF-21-02-076). This work is also partially supported by the XJTLU AI University Re-search Centre, Jiangsu Province Engineering Research Centre of Data Science and Cognitive Computation at XJTLU, and the SIP AI innovation platform (YZCXPT2022103). This project is supported by the National Natural Science Foundation of China (Nos. 62573363 and 62505171). This work also acknowledges Jiangsu Provincial Outstanding Youth Program (BK20230072), Suzhou Industrial Foresight and Key Core Technology Project (SYC2022044), and grants from Jiangsu QingLan Project and Jiangsu 333 high-level talents.

In this paper, we present a 3D biomimetic SERS substrate featuring naturally cone-shaped nanopillars inspired by cicada wings and demonstrate the ability for detecting and differentiating the spectra of common dyes (Fig. 1). We propose a facile, integrated fabrication strategy in which sulfur groups are grafted onto the hydroxyl-rich nanopaper surface to ensure strong binding of AuNPs during transfer printing. This approach eliminates the need for additional complex chemical reactions to generate plasmonic nanostructures on nanopaper. Compared with traditional 2D SERS substrates, the 3D biomimetic architecture exhibits stronger electromagnetic oscillations, as confirmed by COMSOL simulations. As a proof of concept, Rhodamine 6G (R6G) was employed as a SERS example, yielding an exceptionally low limit of detection (LOD, 286 fM) and a high enhancement factor (EF) as $1.09 \times 10^9$. The cone-shaped nanopillars effectively trapped analyte molecules within volumetric hot spots, substantially enhancing Raman signals. Owing to its low cost, reproducibility, and high sensitivity, the proposed biomimetic nanopaper-based SERS substrate holds strong potential for practical chemical and biological sensing applications.

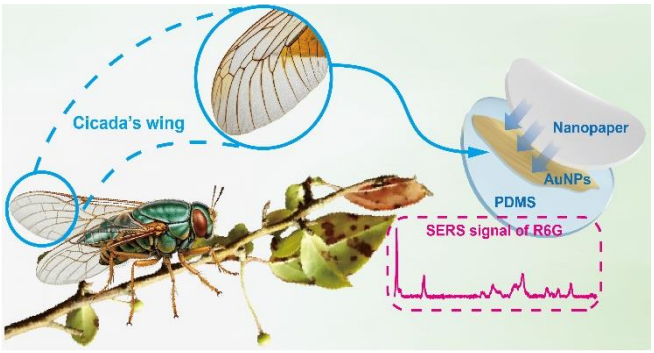


Fig. 1. Schematic illustration of a cicada-wing-inspired nanopaper-based SERS substrate.

## II. Method

### A. Reagents and materials

TEMPO-oxidized nanofibrillated cellulose (NFC) slurry (solid content: 1.0 wt%, carboxylate content: 0.5 mmol/g, average nanofiber diameter: 10 nm) was procured from Tianjin University of Science and Technology (Tianjin, China). Hydrogen tetrachloroaurate(III) trihydrate ($HAuCl_4 \cdot 3H_2O$, ≥ 99.9%) and sodium citrate ($C_6H_5Na_3O_7$, > 98%) were obtained from Aladdin Reagent (Shanghai, China). Rhodamine 6G (R6G) and (3-mercaptopropyl) trimethoxysilane (MPTMS) were purchased from Macklin Biochemical Co., Ltd. (Shanghai, China). A two-part silicone elastomer kit (Sylgard-184, polydimethylsiloxane base and curing agent) was supplied by Dow Corning (Midland, USA). Cicada wings were acquired from a commercial supplier via Alibaba (Shanghai, China).

### B. Preparation of the modified nanopaper

A 4.0 g sample of TEMPO-oxidized NFC slurry was dispersed in distilled water to achieve a concentration of 0.1 wt% and mechanically stirred until homogeneous. The resulting suspension was vacuum-filtered through a polyvinylidene difluoride (PVDF) membrane (VVLP04700, EMD Millipore; 0.1 µm pore size) supported on a glass filter holder, forming a wet, transparent nanopaper gel. After drying, the nanopaper was immersed in an MPTMS solution for three days. During this process, the methoxy groups of MPTMS undergo hydrolysis to form silanol groups, which adsorb onto the hydroxyl groups present on the nanopaper surface via hydrogen bonding. When this functionalized stamp is brought into contact with an MPTMS-based self-assembled monolayer, sulfur–gold bonds form specifically in the contact regions.[25], [26].

### C. Preparation of AuNPs

According to the literature [27], [28], 188.5 mL of an aqueous $HAuCl_4$ solution (0.04%) was placed in a round-bottom flask and heated to boiling under continuous magnetic stirring. Subsequently, 11.5 mL of a trisodium citrate solution ($C_6H_5Na_3O_7 \cdot 2H_2O$, 1%) was added dropwise along a glass rod under vigorous stirring while maintaining boiling. The solution underwent a series of color changes: initially transparent, then turning black, mauve, and finally dark red. Heating and stirring were continued until no further color change was observed. After cooling to room temperature, the resulting AuNP suspension was stored at 4 °C for further use.

### D. Preparation of cicada wing mold coated with AuNPs

The biomimetic silicone mold of cicada wings was fabricated using soft lithography. A silicone elastomer for replicating the cicada wings was prepared from Sylgard 184 (Dow Corning) with a base-to-curing agent ratio of 10:1 [29]. The cicada wings were affixed to a Petri dish, and liquid silicone was poured over them. The dish was then subjected to repeated vacuum cycles in a vacuum oven to remove all bubbles. Subsequently, the silicone was cured at 60 °C for 4 hours. After curing, the silicone replicas were carefully peeled off using tweezers, rinsed with distilled water for 10 minutes, and finally employed as cicada wing replicas. The replica was attached to a glue mixer, and an AuNP solution was spin-coated onto it until a continuous layer fully covered the mold surface.

### E. Preparation of the nanopaper-based SERS substrate

The PDMS molds with cicada wing inspired nanostructures modified by AuNPs were laid up the modified nanopaper and placed between two poly(ethylene terephthalate) films and hot-embossing under at 50 °C and 750 kPa for 10 minutes. After releasing the PDMS molds, the nanopaper with transferred AuNPs was dried at room temperature (Fig. 2).

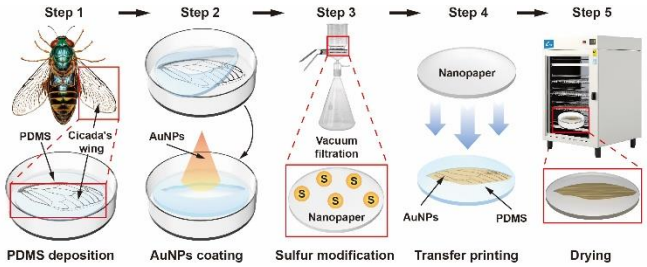


Fig. 2. Fabrication process of a cicada-wing-inspired, nanopaper-based SERS substrate.

### F. SERS measurement

All Raman spectra were measured by a Horiba LabRAM Odyssey Nano Raman equipment (Japan) under a 532 nm laser and selecting 50× objective. $10^{-5}$ to $10^{-12}$ M R6G has dissolved in ethanol. 5 µL aliquot of the above R6G solution with different concentrations was dropped onto the nanopaper and left to dry in the air. The Raman spectra were all recorded

in the range of 600 to 1800 $cm^{-1}$. Each spectrum was obtained as the average of four measurements.

### G. Instrumentation and software

The formation of AuNPs was charactered using a UV-Vis spectrophotometer (Agilent Cary 60, USA).

Transmission electron microscopy (TEM) imaging was performed using a FEI Talos F200X G2 system (USA) operated at an accelerating voltage of 50 kV.

The surface morphologies of the cicada wing, PDMS molds, and the cicada wing-inspired nanopaper-based SERS substrates were examined by scanning electron microscopy (SEM) using an FEI Scios 2 HiVac instrument (USA) at an accelerating voltage of 10 kV.

The same SEM system was equipped with an energy-dispersive X-ray spectroscopy (EDS) detector to analyze the gold nanoparticle (AuNP) content.

The electromagnetic field distribution of AuNPs (40 nm in diameter) on the nanopaper substrate was simulated using COMSOL Multiphysics software (version 6.1, COMSOL Inc., USA).

All spectral data were reorganized by Origin 2022 (OriginLab, USA), and a baseline correction procedure was applied to obtain the final spectrum for each measurement.

## III. Results and Discussion

### A. Enhancement mechanism of the cicada-wing-inspired SERS substrate

A molecule that has been properly isolated can have its Raman spectrum enhanced by many orders of magnitude by nanostructures with sharp edges and small nooks that create hot spots where the local electric field is substantially greater. To further investigation of the the strong Raman enhancement effect of AuNPs on cicada wings-based structure, the electromagnetic field distribution of AuNPs (40 nm in diameter) on the nanopaper substrate was simulated using the COMSOL software (COMSOL 6.1), and two simplified models were constructed, as shown in Fig. 3a and Fig. 3b. The electric field strength was increased, the optical path was lengthened, and light was reflected numerous times between the two parallel nanostructures. Consequently, volume hotspots were dispersed across the two AuNPs@nanostructures that were running parallel to one other, creating 3D optical cavities; also, very strong local hotspots were present, indicating a significant link between dense local hotspots and large-volume hotspots. The monolayer AuNPs@nanostructures' electric field distribution is shown in Fig. 3b. Large-volume hotspots were created and photon energy was efficiently used because the 3D optical cavity was also formed, trapping laser light inside for numerous reflections. Capillary action allowed molecules to pass through the gaps between the AuNPs when the micro-extraction two nanopillars AuNPs@nanostructures was utilized for SERS detection of certain chemical solutions. When these gaps were exposed to laser radiation, volume hotspots developed in them. Because molecules were more likely to become trapped in these hotspots, the Raman signals in these gaps were noticeably amplified, leading to ultrasensitive detection. The electromagnetic enhancement mechanism significantly improves the SERS activity of the substrate, primarily by generating a high density of both lateral and longitudinal "hot spots," which in turn greatly enhances its analytical sensitivity. Although its individual contribution may be limited compared to other mechanisms (e.g., chemical enhancement), its overall impact is substantial. This is because a reduction in the gap between nanostructures causes a pronounced rise in plasmon oscillation intensity. As a result, the enhancement effect grows exponentially as the gap decreases. Although the nano columns transferred onto the nano paper are not as smooth as those in the simulation, small deviations will not have a significant impact on the simulation results. In addition, simulation experiments are only conducted on a large number of general models. Moreover, it is important to observe that the electromagnetic enhancement factor that the COMSOL program simulates is not the same as the real one. This problem is caused by the fact that the surface of the actual nanopillars is not as uniform as the surface used for convenience in COMSOL simulation. We have demonstrated the cause of the Raman scattering signal augmentation in the theoretical simulation section, and the experimental and theoretical simulation results are in good agreement.

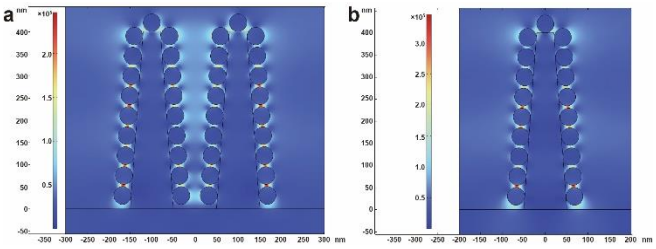


Fig. 3. Simulated electric-magnetic field distributions of cicada wing inspired nannopillars: (a) between two AuNPs@nanostructure nanopillars and (b) on a single AuNPs@nanostructure nanopillar.

### B. Characterization of cicada wing-inspired nanopaper-based SERS substrate

Using naturally occurring raw materials to produce large-area arrays of vertically aligned nanopillars from a cicada wing significantly lowers the production costs of SERS substrates. This method can be directly utilized as a 3D substrate template, significantly simplifying the complex experimental procedures typically involved in template fabrication. To verify the successful preparation of the cicada-wing-inspired nanopaper-based SERS substrate, several characterization techniques were employed. Initially, UV–Vis spectra of AuNPs with varying sizes were obtained. As illustrated in Fig. 4a, surface plasmon resonance (SPR absorption peaks were observed at 525 nm and 530 nm, corresponding to AuNPs with average sizes of approximately 30 nm and 40 nm, respectively. In our previous study, highly uniform and well-ordered AuNP arrays were fabricated, demonstrating an average particle diameter of 40 ± 4.78 nm. The well-defined architecture of the SERS substrate also plays a crucial role in enabling high detection sensitivity. Side-view SEM images of cicada wings, PDMS molds with AuNPs, and the transferred nanopaper substrate are presented in Figs. 4b–4d, respectively. The nanopillars on cicada wing (Fig. 4b) have a circular base with a radius of 160 nm, a circular top with a radius of 70 nm, and the height of the nanopillars occurring as 400 nm. These nanopillars possess a unique morphology featuring a cone-shaped top, a broader spacing near the top, and a narrower spacing near the base. It is well established that 3D SERS-active substrates generate many more hotspots than 1D and 2D substrates, which is crucial for producing strong electric-magnetic enhancement. The uniform nanopillars also provide a larger surface area,

facilitating the deposition of noble metals' nanoparticles and the adsorption of analytes. An SEM image of the PDMS mold with AuNPs is shown in Fig. 4c. The nanopillars on the mold have a circular base with a radius of 180 nm, a circular top with a radius of 55 nm, and the height stilling of 400 nm. The 180 nm gaps between nanopillars are decorated with AuNPs. The transferred nanopaper-based SERS substrate (Fig. 4d) retains the uniform nanopillar structure of the cicada wing, with AuNPs surrounding the nanopillars, confirming the successful fabrication of the SERS substrate.

Photographs of the PDMS mold and the nanopaper substrate are shown in Figs. 4e and 4f, where the texture of the cicada wing is clearly visible on both the PDMS mold and the transferred nanopaper substrate. The AuNP layer is also evident on the nanopaper bearing the cicada wing texture, confirming the successful fabrication of the SERS substrate. The transfer percentage was defined as the mass difference between the PDMS mold with AuNPs and the PDMS mold after transfer, divided by the mass difference between the PDMS mold with AuNPs and the pristine PDMS mold.

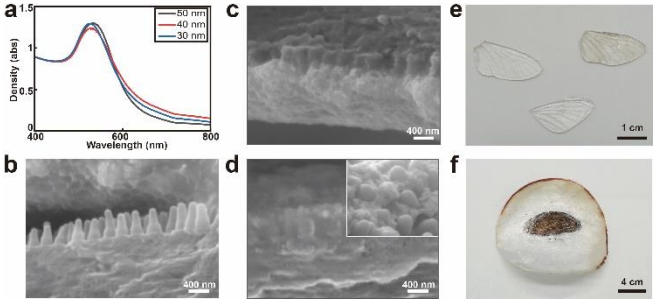


Fig. 4. Characterization of the cicada-wing-inspired nanopaper-based SERS substrate. (a) UV–Vis spectra of AuNPs. (b) SEM photo of a cicada wing. (c) SEM photo of a PDMS mold decorated with AuNPs. (d) SEM image of the cicada-wing-inspired nanopaper-based SERS substrate. Photographs of (e) PDMS molds and (f) the cicada-wing-inspired nanopaper-based SERS substrate.

To evaluate the transfer efficiency, the PDMS molds were equally divided into two parts, and one part was used for transfer onto the nanopaper. The pristine PDMS molds exhibited distinct gold (Au), carbon (C), and oxygen (O) peaks under the same magnification. The elemental compositions are summarized in Table I. The Au content before and after transfer printing was 89.00 ± 2.80 wt% and 9.69 ± 7.18 wt%, respectively (n = 3). The difference in Au content before and after transfer printing was 79.30 ± 4.38 wt%, corresponding to a transfer efficiency of 89.27 ± 6.43%, demonstrating the high accuracy of the method developed in this study.

TABLE I. DISTRIBUTION CHART TOTAL NUMBER SPECTRUM OF PDMS MOLDS BEFORE AND AFTER TRANSFER PRINTING

| Elements | Sample 1 (I) | Sample 1 (II) | Sample 2 (I) | Sample 2 (II) | Sample 3 (I) | Sample 3 (II) |
|---|---|---|---|---|---|---|
| C wt% | 7.35 | 44.44 | 10.48 | 32.02 | 7.80 | 55.85 |
| O wt% | 1.75 | 40.94 | 3.74 | 66.53 | 1.91 | 33.14 |
| Au wt% | 90.91 | 14.62 | 85.78 | 1.45 | 90.29 | 13.01 |
| All wt% | 100 | 100 | 100 | 100 | 100 | 100 |
| D-value wt% | | 76.29 | | 84.33 | | 77.28 |
| Efficiency % | | 83.92 | | 98.31 | | 85.59 |

### C. *SERS-based determination of carcinogenic molecules on transferred nanopaper-based substrates*

Previous studies have shown that aggregated AuNPs can significantly enhance SERS signal intensity, even downing to the detection of individual molecules. However, the formation of plasmonic near-field hotspots typically occurs in an uncontrolled manner, resulting in uneven distribution and low spatial density. The radius of AuNPs therefore plays a critical role in SERS performance. Fig. 5a and 5c show the SERS signal enhancement obtained with AuNPs of different diameters (30 nm and 40 nm) on 3D nanopaper-based substrate. The 40 nm AuNPs produced higher signal intensity than the 30 nm AuNPs. The presence of analytes can also influence nanoparticle behavior in solution through the formation of small aggregates. Theoretically, the extinction spectra of AuNPs exhibit an increasing contribution from multipole absorption as particle size increases, leading to a broadening and redshift of the plasmon band [30]. The higher SERS intensity observed with larger AuNPs in this study can be attributed to the combined effects of higher-order plasmon modes and the greater magnitude of electromagnetic (EM) field enhancement around larger nanoparticles [31]. It is worth noting that the optimal particle size for SERS is only applicable when the analyte concentration surpasses the requirement of received monolayer coverage of the nanoparticles; larger particles are less effective for detecting low analyte concentrations [32]. Based on these considerations, 40 nm AuNPs were selected for the subsequent fabrication of the transferred cicada-wing-inspired nanopaper-based SERS substrate.

R6G was dissolved in ethanol, and a 5 μL aliquot of the resulting solution was drop-cast onto the functionalized region of the nanopaper substrate for Raman analysis. Figure 5d displays the Raman spectra of R6G across a concentration range from 10 μM down to 1 pM, with pure ethanol used as a blank control. The characteristic Raman peaks of R6G are clearly visible, including bands associated with C–C ring bending (610 $cm^{-1}$), C–H out-of-plane bending (774 $cm^{-1}$), C–H bending (935 $cm^{-1}$), C–O–C stretching (1184 and 1282 $cm^{-1}$), and aromatic C–C stretching (1310, 1364, 1508, 1578, and 1648 $cm^{-1}$).The peak at 610 $cm^{-1}$ was selected for quantitative analysis due to its high sensitivity to R6G concentration and minimal background interference. A calibration curve constructed based on this peak is presented in Fig. 5e. The limit of detection (LOD) was determined to be 286 fM, calculated as the concentration corresponding to the signal intensity of the blank control plus three times its standard deviation. The observed variability in SERS intensities, as indicated by the error bars, confirms that this method is a highly feasible and selective approach for the sensitive detection of carcinogenic molecules.

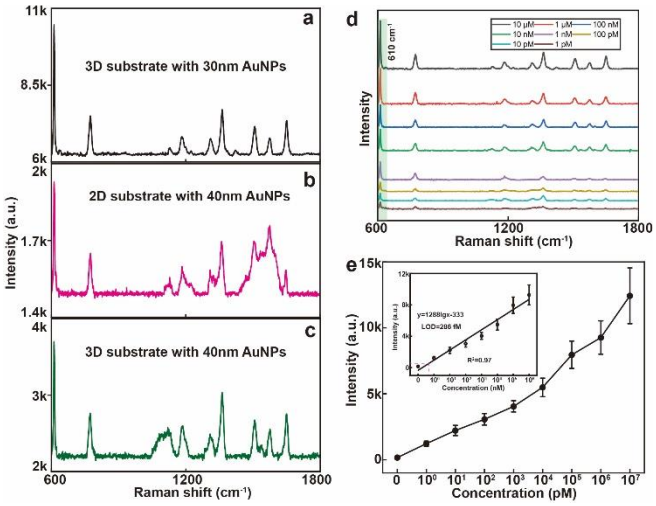


Fig. 5. Presentation of the Raman detection results of Rhodamine 6G (R6G). (a) and (c) show the Raman spectra of R6G at a concentration of $10^{-5}$ M deposited on cicada wing-inspired nanopaper-based SERS substrates decorated with 30 nm and 40 nm Au nanoparticles, respectively. (b) displays the corresponding spectra obtained using a plate-transferred nanopaper-based SERS substrate under the same analyte concentration. (d) Illustration of the Raman spectra of R6G at various concentrations ranging from $10^{-5}$ M to $10^{-12}$ M. (e) Showing the corresponding calibration curve derived from the measurements (n = 4).

The comparative Raman intensities of R6G on AuNP-transferred nanopaper substrates without the cicada-wing micro/nanostructure (control substrate) are shown in Fig. 5b. $10^{-5}$ M R6G solution was selected as an example for the comparison between the 3D and 2D SERS substrate. The cicada-wing-inspired nanopaper-based SERS substrate exhibited nearly five times higher intensity than the flat control substrate, clearly demonstrating that the biomimetic surface provides greater enhancement than a smooth surface. On flat substrates lacking topographical features, nanoparticles tend to remain conformal and are less likely to aggregate, resulting in lower hotspot density and weaker Raman enhancement. In contrast, the hierarchical micro/nanostructures on the transferred nanopaper-based SERS substrate promote adsorption and local concentration of analyte molecules on dense AuNP aggregates, producing stronger SERS signals. Structural parameters such as feature shape, height, aspect ratio, and spacing are critical to the performance of micro/nanostructures. Compared with non-structured surfaces, micro/nanostructures enhance light scattering and confine nanoparticles in interstitial regions, generating hotspots. Therefore, the distinct architecture of the biomimetic substrate promotes AuNP aggregation, increasing light trapping and improving optical coupling.

The intensity of R6G was another important factor for calculating the Raman EF to comprehensively evaluate the SERS activity of this 3D substrate. The EF was determined from the R6G example resulting as:

$$EF = \frac{I_{SERS}}{I_{bare}} \times \frac{C_{bare}}{C_{SERS}} \quad (1)$$

where $I_{SERS}$ and $C_{SERS}$ are the Raman intensity at 610 cm$^{-1}$ and the concentration on the transferred nanopaper substrate, respectively. $I_{bare}$ and $C_{bare}$ are the corresponding values for bare nanopaper. The calculated EF was $1.09\times10^{9}$, which is comparable to other inorganic semiconductor and noble-metal-based SERS substrates, confirming the high SERS sensitivity toward R6G.

Several factors contribute to this outstanding performance. First, nanopaper offers superior optical transparency compared with regular paper, minimizing signal loss from light reflection (the LOD for *in situ* AuNP-functionalized regular paper is only ~0.8 mM). Second, the fabrication of the nanopaper-based substrate is a highly integrated and straightforward process, reducing the risk of contamination during manufacturing. Third, the total EF is enhanced by a combination of light scattering from the micro/nanostructures and nanoparticle assembly. The affinity of R6G molecules for the AuNP surface allows for more efficient adsorption, while the substrate design promotes the formation of homogeneous nanojunctions, similar to effects reported for plant leaf-based SERS substrates. Under laser excitation, the 3D optical cavities formed between nanopillars enhance plasmon resonance coupling and confine light, significantly boosting Raman signals. These results illustrating the nanopaper-based SERS substrate has strong potential for ultrasensitive detection of various analytes.

## IV. Conclusion

In this work, we demonstrated the fabrication of easy, low-cost, high-effective and reproducible nanopaper-based SERS substrates inspired by cicada wing biomimetic surfaces via a transfer printing method. A simple functionalization of the nanopaper surface was performed to enhance the efficiency of AuNP transfer. Using soft lithography, the naturally occurring microstructures of cicada wings were replicated and subsequently employed to assemble AuNPs in a distinctive arrangement, generating abundant electromagnetic hotspots. R6G was employed as a model Raman reporter to validate the feasibility of the design, achieving an LOD of 286 fM and a Raman EF of $1.09 \times 10^{9}$. Comparison between the biomimetic nanopaper-based SERS substrates and regular transferred nanopaper revealed that the superior SERS performance of the former is directly correlated with the unique surface morphology and ordered microstructure arrangement. These cicada-wing-inspired biomimetic SERS substrates demonstrate high efficiency, low production cost, and excellent reproducibility. Coupled with strategically designed SERS-active layers, they hold strong potential for label-free and simple detection with high sensitivity of various chemicals and biomarkers.

## Acknowledgment

All authors have given approval to the final version of the manuscript.

## References

[1] E. Morales-Narváez *et al.*, 'Nanopaper as an Optical Sensing Platform', *ACS Nano*, vol. 9, no. 7, pp. 7296–7305, Jul. 2015, doi: 10.1021/acsnano.5b03097.

[2] H. Zhu, Z. Fang, C. Preston, Y. Li, and L. Hu, 'Transparent paper: fabrications, properties, and device applications', *Energy Environ. Sci.*, vol. 7, no. 1, pp. 269–287, Dec. 2013, doi: 10.1039/C3EE43024C.

[3] M. Nogi, S. Iwamoto, A. N. Nakagaito, and H. Yano, 'Optically Transparent Nanofiber Paper', *Adv. Mater.*, vol. 21, no. 16, pp. 1595–1598, 2009, doi: 10.1002/adma.200803174.

[4] H. Yuan *et al.*, 'Centrifugation-assisted lateral flow assay platform: enhancing bioassay sensitivity with active flow control', *Microsyst. Nanoeng.*, vol. 11, no. 1, p. 101, May 2025, doi: 10.1038/s41378-025-00923-5.

[5] A. Dufresne, 'Nanocellulose: a new ageless bionanomaterial', *Mater. Today*, vol. 16, no. 6, pp. 220–227, Jun. 2013, doi: 10.1016/j.mattod.2013.06.004.

[6] F. J. Martin-Martinez, 'Designing nanocellulose materials from the molecular scale', *Proc. Natl. Acad. Sci.*, vol. 115, no. 28, pp. 7174–7175, Jul. 2018, doi: 10.1073/pnas.1809308115.

[7] R. R. Jones, D. C. Hooper, L. Zhang, D. Wolverson, and V. K. Valev, 'Raman Techniques: Fundamentals and Frontiers', *Nanoscale Res. Lett.*, vol. 14, no. 1, p. 231, Jul. 2019, doi: 10.1186/s11671-019-3039-2.

[8] L. Chen, B. Ying, P. Song, and X. Liu, 'A Nanocellulose-Paper-Based SERS Multiwell Plate with High Sensitivity and High Signal Homogeneity', *Adv. Mater. Interfaces*, vol. 6, no. 24, p. 1901346, 2019, doi: 10.1002/admi.201901346.

[9] B. Ying, S. Park, L. Chen, X. Dong, E. W. K. Young, and X. Liu, 'NanoPADs and nanoFACEs: an optically transparent nanopaper-based device for biomedical applications', *Lab. Chip*, vol. 20, no. 18, pp. 3322–3333, Sep. 2020, doi: 10.1039/D0LC00226G.

[10] W. Yuan *et al.*, 'Facile Microembossing Process for Microchannel Fabrication for Nanocellulose-Paper-Based Microfluidics', *ACS Appl. Mater. Interfaces*, vol. 15, no. 5, pp. 6420–6430, Feb. 2023, doi: 10.1021/acsami.2c19354.

[11] W. Yuan *et al.*, 'Metal–Organic Frameworks/Heterojunction Structures for Surface-Enhanced Raman Scattering with Enhanced Sensitivity and Tailorability', *ACS Appl. Mater. Interfaces*, May 2024, doi: 10.1021/acsami.4c01588.

[12] J. Zaumseil *et al.*, 'Three-Dimensional and Multilayer Nanostructures Formed by Nanotransfer Printing', *Nano Lett.*, vol. 3, no. 9, pp. 1223–1227, Sep. 2003, doi: 10.1021/nl0344007.

[13] Y.-L. Loo, R. L. Willett, K. W. Baldwin, and J. A. Rogers, 'Interfacial Chemistries for Nanoscale Transfer Printing', *J. Am. Chem. Soc.*, vol. 124, no. 26, pp. 7654–7655, Jul. 2002, doi: 10.1021/ja026355v.

[14] J. W. Jeong *et al.*, 'High-resolution nanotransfer printing applicable to diverse surfaces via interface-targeted adhesion switching', *Nat. Commun.*, vol. 5, no. 1, p. 5387, Nov. 2014, doi: 10.1038/ncomms6387.

[15] W. Wu *et al.*, 'Low-Cost, Disposable, Flexible and Highly Reproducible Screen Printed SERS Substrates for the Detection of Various Chemicals', *Sci. Rep.*, vol. 5, no. 1, p. 10208, May 2015, doi: 10.1038/srep10208.

[16] Y. Xu *et al.*, 'Screen-Printable Thin Film Supercapacitor Device Utilizing Graphene/Polyaniline Inks', *Adv. Energy Mater.*, vol. 3, no. 8, pp. 1035–1040, Aug. 2013, doi: 10.1002/aenm.201300184.

[17] J. P. Metters, S. M. Houssein, D. K. Kampouris, and C. E. Banks, 'Paper-based electroanalytical sensing platforms', *Anal. Methods*, vol. 5, no. 1, pp. 103–110, Dec. 2012, doi: 10.1039/C2AY26396C.

[18] X. Huang *et al.*, 'Controllable self-assembled plasmonic vesicle-based three-dimensional SERS platform for picomolar detection of hydrophobic contaminants', *Nanoscale*, vol. 10, no. 27, pp. 13202–13211, Jul. 2018, doi: 10.1039/C8NR02778A.

[19] C. Zhang *et al.*, 'SERS activated platform with three-dimensional hot spots and tunable nanometer gap', *Sens. Actuators B Chem.*, vol. 258, pp. 163–171, Apr. 2018, doi: 10.1016/j.snb.2017.11.080.

[20] J. Chen *et al.*, 'Nanoimprinted Patterned Pillar Substrates for Surface-Enhanced Raman Scattering Applications', *ACS Appl. Mater. Interfaces*, vol. 7, no. 39, pp. 22106–22113, Oct. 2015, doi: 10.1021/acsami.5b07879.

[21] X. Xie, H. Pu, and D.-W. Sun, 'Recent advances in nanofabrication techniques for SERS substrates and their applications in food safety analysis', *Crit. Rev. Food Sci. Nutr.*, vol. 58, no. 16, pp. 2800–2813, Nov. 2018, doi: 10.1080/10408398.2017.1341866.

[22] N. Zhao *et al.*, 'Bioscaffold arrays decorated with Ag nanoparticles as a SERS substrate for direct detection of melamine in infant formula', *RSC Adv.*, vol. 9, no. 38, pp. 21771–21776, 2019, doi: 10.1039/C9RA01862J.

[23] F. Shao *et al.*, 'Hierarchical Nanogaps within Bioscaffold Arrays as a High-Performance SERS Substrate for Animal Virus Biosensing', *ACS Appl. Mater. Interfaces*, vol. 6, no. 9, pp. 6281–6289, May 2014, doi: 10.1021/am4045212.

[24] M. Y. Lv *et al.*, 'Low-cost Au nanoparticle-decorated cicada wing as sensitive and recyclable substrates for surface enhanced Raman scattering', *Sens. Actuators B Chem.*, vol. 209, pp. 820–827, Mar. 2015, doi: 10.1016/j.snb.2014.12.061.

[25] B. Fathi, M. Harirforoush, Mr. Foruzanmehr, S. Elkoun, and M. Robert, 'Effect of TEMPO oxidation of flax fibers on the grafting efficiency of silane coupling agents', *J. Mater. Sci.*, vol. 52, no. 17, pp. 10624–10636, Sep. 2017, doi: 10.1007/s10853-017-1224-1.

[26] M. Hu, S. Noda, T. Okubo, Y. Yamaguchi, and H. Komiyama, 'Structure and morphology of self-assembled 3-mercaptopropyltrimethoxysilane layers on silicon oxide', *Appl. Surf. Sci.*, vol. 181, no. 3, pp. 307–316, Sep. 2001, doi: 10.1016/S0169-4332(01)00399-3.

[27] G. Frens, 'Controlled Nucleation for the Regulation of the Particle Size in Monodisperse Gold Suspensions', *Nat. Phys. Sci.*, vol. 241, no. 105, Art. no. 105, Jan. 1973, doi: 10.1038/physci241020a0.

[28] B. Xue *et al.*, 'An AuNPs/Mesoporous NiO/Nickel Foam Nanocomposite as a Miniaturized Electrode for Heavy Metal Detection in Groundwater', *Engineering*, Jul. 2022, doi: 10.1016/j.eng.2022.06.005.

[29] M. Barshutina *et al.*, 'SERS substrates based on rose petal replicas for the oxidative stress detection', *Appl. Surf. Sci.*, vol. 626, p. 157281, Jul. 2023, doi: 10.1016/j.apsusc.2023.157281.

[30] K. L. Kelly, E. Coronado, L. L. Zhao, and G. C. Schatz, 'The Optical Properties of Metal Nanoparticles: The Influence of Size, Shape, and Dielectric Environment', *J. Phys. Chem. B*, vol. 107, no. 3, pp. 668–677, Jan. 2003, doi: 10.1021/jp026731y.

[31] K. G. Stamplecoskie, J. C. Scaiano, V. S. Tiwari, and H. Anis, 'Optimal Size of Silver Nanoparticles for Surface-Enhanced Raman Spectroscopy', *J. Phys. Chem. C*, vol. 115, no. 5, pp. 1403–1409, Feb. 2011, doi: 10.1021/jp106666t.

[32] K. Tanabe, 'Field Enhancement around Metal Nanoparticles and Nanoshells: A Systematic Investigation', *J. Phys. Chem. C*, vol. 112, no. 40, pp. 15721–15728, Oct. 2008, doi: 10.1021/jp8060009.